

Kinetics and Mechanisms of Pb(II) Sorption and Desorption at the Aluminum Oxide–Water Interface

DANIEL G. STRAWN,^{*,†}
ANDRÉ M. SCHEIDEGGER,[‡] AND
DONALD L. SPARKS[†]

Department of Plant and Soil Sciences, University of Delaware, Newark, Delaware 19717-1303, and Waste Management Laboratory, Paul Scherrer Institut, CH-5232 Villigen PSI, Switzerland

The fate of Pb in the environment is highly dependent on sorption and desorption reactions on solid surfaces. In this study Pb sorption and desorption kinetics on γ -Al₂O₃ at pH 6.50, $I = 0.1$ M, and [Pb]_{initial} = 2 mM were investigated using both macroscopic and spectroscopic measurements. X-ray absorption fine structure (XAFS) spectroscopy revealed a Pb–Al bond distance of 3.40 Å, consistent with an inner-sphere bidentate bonding mechanism. XAFS results show no change with time in the average local atomic structure surrounding the Pb and no indication of the formation of Pb surface precipitates. Adsorption kinetics were initially fast, resulting in 76% of the total sorption occurring within 15 min, followed by a slow continuous sorption reaction likely resulting from diffusion through micropores. Desorption at $I = 0.1$ M and pH 6.50 was studied using a cation-exchange resin as a sink for Pb(aq). Under these conditions, Pb desorption was 98% reversible within 3 days of incubation time. Furthermore, desorption and adsorption kinetics demonstrated similar trends: a fast reaction followed by a slow reaction. The use of spectroscopy combined with adsorption and desorption kinetic studies has revealed important information on the interaction between lead and aluminum (hydr)oxides. This information is valuable for predicting the fate of Pb in the environment.

Introduction

The reaction of metals at the solid–solution interface plays an important role in determining their fate in the environment. In the past, researchers have focused on determining adsorption distribution coefficients (K_d), sorption capacity, and the pH dependence of metal sorption. Often these studies were based on short reaction periods, for example, 24 h. However, in natural systems reactions can continue for days, months, or years (1–4). In addition, researchers often neglect desorption reactions, assuming that sorption and desorption rates are the same. However, desorption can often be much slower, and sorption reactions are often nonreversible (5). This may be a reason for the commonly observed hysteresis (6).

Metal sorption at the mineral–water interface is often initially fast followed by a decrease in the sorption rate

(3, 5, 7–12). Three possible mechanisms for the slow reactions have been proposed: diffusion into micropores of solids, followed by sorption to interior sites; sorption to sites of lower reactivity; and surface precipitation (3, 9, 11, 13–15). Distinguishing between these mechanisms based on macroscopic experiments alone is difficult. One approach used to address these difficulties is to investigate sorption mechanisms using spectroscopy that allows reactions to be studied at a molecular level.

In the past several years, the use of X-ray absorption spectroscopy (XAS) to study Pb sorption reactions has provided important mechanistic information (16–21). Bargar et al. (20) studied Pb sorption on α -Al₂O₃ (corundum). They concluded that the Pb sorption mechanism was primarily bidentate edge-sharing complexes (inner-sphere). Bargar et al. (18) also used grazing incident XAS and found that Pb formed outer-sphere bonds on the 0001 plane of α -Al₂O₃. This research has provided evidence that Pb sorption is heterogeneous and involves several different mechanisms. Since the sorption mechanisms vary, it is likely that the rates of the sorption mechanisms are different, and there may be slow reactions that are not measured under short reaction periods. Thus, in this study we have expanded the investigation of Pb sorption mechanisms on aluminum (hydr)oxides by combining kinetic and spectroscopic measurements so that possible changes in reaction mechanisms can be distinguished.

The combination of kinetics and spectroscopy to do real time sorption studies (time-resolved) is ideal since spectroscopy can provide direct information on the type of species present at the surface and kinetics can provide insight into the processes that the sorbate and sorbent undergo to reach equilibrium (4, 12, 22–25). Scheidegger et al. (12) combined kinetics and XAS and showed that the formation of mixed nickel/aluminum hydroxide surface precipitates was one of the mechanisms responsible for slow Ni sorption on montmorillonite. To date, the formation of mixed precipitates has not been observed as a sorption mechanism for Pb sorption on aluminum (hydr)oxides over relatively short time periods. The formation of a solid solution is not likely since the radius of Pb is too large to substitute for Al in a mineral structure (20, 26). However, surface precipitates may occur in systems that are undersaturated with respect to the (hydr)oxide species (15). Since precipitation is often a slower process than adsorption and the surface can affect solubility constants, precipitation has not been ruled out as a possible sorption mechanism for Pb on γ -Al₂O₃ in samples incubated for extended times.

The objectives of this study were to investigate the kinetics and mechanisms of Pb sorption and desorption on γ -Al₂O₃ over incubation periods longer than the traditional 24 h, including sorption reversibility, and the stability of sorbed Pb. Both macroscopic kinetic experiments and time-resolved XAFS measurements were conducted. The information presented in this study will provide insights into the mechanisms of Pb sorption on γ -Al₂O₃ that are relevant to the long exposure times that exist in the environment and will help with modeling Pb sorption reactions on mineral surfaces.

Aluminum minerals play an important role in the sequestration and immobilization of trace elements in the environment (27). They possess amphoteric surface aluminol functional groups that form chemical bonds with many heavy metals, including Pb (27–30). In nature, γ -Al₂O₃ is found only under high pressure and high temperature conditions. However, the surface of this mineral completely hydrates

* Corresponding author e-mail: dgstrawn@Ude.edu; fax: (302)-831-0605; telephone: (302)831-1595.

[†] University of Delaware.

[‡] Paul Scherrer Institut.

when exposed to moisture, creating a layer of chemisorbed water along the basal plane of the mineral (27, 31, 32). Thus, the hydrated surface of γ -Al₂O₃ is similar to aluminum hydroxide minerals commonly found in soils, such as gibbsite, bayerite, and boehmite. Therefore, γ -Al₂O₃ is a useful mineral for simulating reactive surfaces occurring in the environment.

Experimental Methods

Materials. The mineral γ -Al₂O₃ was obtained from Degussa Inc. (Akron, OH). Other than freeze-drying for accurate weight measurements, the γ -Al₂O₃ was used as received. The γ polymorph of Al₂O₃ is a synthetic mineral. It is ideal for experimental work since it is well characterized, it can be commercially obtained in a relatively pure state (greater than 99.6% is Al₂O₃, structure confirmed by X-ray diffraction), and it has a large surface area (~ 100 m² g⁻¹) allowing for a high metal loading level that is necessary for spectroscopic (XAFS) measurements.

All solutions were made with ACS reagent grade chemicals and distilled deionized (D.I.) H₂O. To eliminate CO₂, all experiments were conducted in a glovebox with an N₂ atmosphere. Temperature was maintained at 25° C.

Sorption Kinetics Experiments. Prior to the addition of the Pb solution, a suspension of 13.3 g L⁻¹ of the γ -Al₂O₃ was pre-equilibrated for 24 h at pH 6.50 in background electrolyte (stirring at 350 rpm). The background electrolyte solution consisted of a mixture of NaNO₃ and 0.075 M MES [2-(*N*-morpholino)ethane sulfonic acid] adjusted to pH 6.50 and total $I = 0.1$ M. MES is an organic buffer with a pK_a of 6.10. It has been shown that this buffer does not significantly complex with metals or interfere with metal sorption (33, 34). At the start of the kinetic experiment, 10-mL aliquots from an 8 mM Pb stock solution ($I = 0.1$ adjusted with NaNO₃) were added every 30 s until the [Pb] = 2 mM and the [γ -Al₂O₃] = 10 g L⁻¹ (total suspension volume = 0.180 L). The suspension pH was then readjusted to pH 6.50 with ~ 20 - μ L drops of 10 M NaOH. To avoid local oversaturation, the very small drops were added while the suspension was being rapidly stirred. Periodically, 5-mL samples were removed and immediately centrifuged at 11950g for 3 min. The supernatant was filtered through a 0.2- μ m filter and acidified with one drop (~ 20 μ L) of concentrated HNO₃. The solution was then analyzed by inductively coupled plasma emission spectrometry (ICP) for total Pb. The amount of Pb sorbed was calculated from the difference between the initial and the final Pb concentration. During the first 24 h of the sorption experiment, the suspension was stirred at 350 rpm with a Teflon stir bar, and subsequently the suspension was placed on an orbital shaker operating at a speed of 150 orbits min⁻¹. The sorption kinetics results represent data points from three separate experiments.

Desorption Experiments. Desorption experiments were carried out using two different methods. In both methods desorption was started after 48 h of sorption incubation time. This reaction time was chosen because the sorption reaction is >97% complete within this time. For the first method, 10 mL of the reacted suspension was centrifuged at 26890g for 5 min. The supernatant was removed and replaced with 9.5 mL of buffered background electrolyte ($I = 0.1$ M, NaNO₃ + MES, pH 6.50). The supernatant was collected and analyzed for total Pb. The total amount of desorbed Pb was calculated by subtracting the nonsorbed Pb entrapped in the paste (left over from the previous replenishment) from the total amount of Pb in solution. This replenishment was carried out every 24 h for 9 days. For the second method, a 5-mL aliquot of the reacted suspension was placed in a 10-mL centrifuge tube with 0.25 g of Dowex-HCR-42 Na saturated (16–40 mesh) cation-exchange resin. The exchange capacity of the resin was 2.4 times greater than the total amount of Pb present in solution and on the sorbent. Periodically, samples were

centrifuged, and the supernatant was collected. Analysis of the supernatant solutions indicated that [Pb] was less than 5 μ M (0.5% initial [Pb]). The resin was separated from the γ -Al₂O₃ by rinsing with D.I. H₂O over an 80 mesh sieve until the resin returned to its translucent color, suggesting that all of the solid (white color) had been removed from the resin. Finally, the resin was placed in a centrifuge tube with 5 mL of 7 M HCl for 24 h to recover the Pb. The amount of Pb remaining on the surface at a given time was calculated as the difference between the initial amount of Pb added to the suspension minus the amount of Pb recovered from the resin. The following observations were made regarding the reliability of the resin desorption method from independent experiments on a 2 mM Pb solution: (1) the resin removed >99% of the Pb from solution; (2) the acid recovered 97% of the total Pb; and (3) the amount of Pb removed from the resin by washing with D.I. H₂O was below detection limits. Corrections were made to the desorption samples for observation 2.

Synchrotron XAS Analysis. Samples analyzed by XAS were prepared independently of the sorption kinetic studies. All experimental conditions were the same except that pH was maintained at 6.50 by the addition of 0.1 M base rather than MES. Samples incubated for 1.5 and 6.5 h were prepared adjacent to the beamline with N₂ rapidly bubbling through the samples to eliminate CO₂. The wet γ -Al₂O₃ pastes were loaded into an Al sample holder and sealed in front and back with Kapton tape (CHR Industries). All samples were immediately cooled to 77 K by placing them in liquid N₂.

XAS data acquisition of the Pb L_{III}-edge (13055) was conducted on beamline X-11A at the National Synchrotron Light Source (NSLS), Brookhaven National Laboratory, Upton, NY. The electron beam energy was 2.5 GeV, and the maximum beam current was 300 mA. The monochromator used in this case consisted of two parallel Si(111) crystals with an entrance slit of 1 mm. The parallel crystal monochromator was detuned by reducing I_0 25% at the Pb-edge. The XAS data were collected in fluorescence mode using a Stern-Heald-type detector filled with Kr and equipped with an As filter (35).

The XAFS data analysis was accomplished using the program MacXAFS 4.0 (36). The XAFS spectra were processed using the following procedure: (1) Multiple scans were merged and normalized relative to E_0 (determined from the inflection point of the derivative of the spectra) and step height; (2) the χ function was extracted from the raw data using a linear pre-edge and a cubic spline post-edge consisting of 3 knots set at unequal distances and converting the data from energy to k space; (3) the χ function was then weighted by k^3 in order to compensate for dampening of the XAFS amplitude with increasing k ; (4) the data were Fourier transformed ($\Delta k = 3.6$ – 11.3 Å⁻¹) to yield a radial structure function (RSF). For background removal (step 2), the positions of the knots were selected using the following criteria: (1) minimization of peaks in the region prior to the first major peak in the RSF, (2) minimization of oscillations in the spline derivative and ensuring nonconformity in oscillation phase between the spline derivative and spectra, and (3) maximizing the height of the primary O peak in the RSF without significantly dampening any other peaks. Once an optimum set of parameters was determined, all sample spectra were processed in the same manner.

The XAFS k^3 weighted spectra were fit in R-space using the fitting routine in MacXAFS 4.0 (36). Background on the theories and procedures for fitting XAFS data can be found elsewhere (37). The particular details used in fitting the data are listed below. Single scattering theoretical spectra and phase shifts for Pb–Pb backscatters, Pb–O backscatters, and Pb–Al backscatters were calculated using the FEFF6.0 code (38), with an input file based on a model of α -PbO

TABLE 1. Structural Parameters for Pb Adsorption on γ -Al₂O₃ Samples Reacted for Different Lengths of Time and α -PbO Derived from the Best-Fit Results of the XAFS Experimental Data with Theoretical Phase Shift and Amplitude Functions

reaction time	Pb–O shell				Pb–Al Shell		
	E_0^a	R (Å) ^{b,e}	$N^{c,f}$	σ^2 (Å ²) ^d	R (Å) ^e	N^g	σ^2 (Å ²) ^h
1.5 h	0.61	2.30	1.9	0.0051	3.43	1.1	0.009
6.5 h	2.75	2.29	2.1	0.0069	3.39	0.9	0.009
25 h	4.28	2.29	2.0	0.0056	3.40	1.0	0.009
42 h	4.25	2.28	1.9	0.0052	3.38	1.1	0.009
23 d	5.71	2.28	2.2	0.0069	3.38	0.9	0.009
α -PbO ⁱ	2.70	2.28	4.1	0.0030	3.67/3.90 ^j	6.2/4.0 ^j	0.006 ^k

^a Phase shift. ^b Interatomic distance. ^c Coordination number. ^d Debye–Waller factor. ^e Fit quality confidence limits for parameters: $\pm 1\%$, $\pm 20\%$, and $\pm 40\%$. ^f Fixed. ^g Fit with three backscattering atoms: O, Pb, and Pb. ^h Slash is a demarcation between Pb backscatterers. ^k Constrained to be equal for both Pb atoms.

(tetrahedral) (39) (generated with the program ATOMS) with two of the Pb atoms at 3.69 Å replaced by Al. The values of the Debye–Waller (σ^2) term for the second shell were fixed at 0.009 Å², which is the average of the σ^2 values from all sorption samples when they were allowed to vary on their own. This is justified by the following observations: when allowed to vary, the standard deviation of the σ^2 was small (0.003 Å²) for all samples; there was no trend in the σ^2 for the samples incubated for different times; fixing the σ^2 reduced the number of free parameters in the fitting routine and thus the uncertainties in the coordination number (N); and, 0.009 Å² is consistent with the value used by other researchers to fit Pb sorption data (16, 20). The edge shift (E_0) for all shells was constrained to be equal. All other parameters were allowed to vary. An amplitude reduction factor was determined by fitting the theoretical single scattering O-shell to the same shell of the experimental spectra of a well-characterized α -PbO. For both the experimental and theoretical spectra, square windows were cut at equal values in the RSF. Based on a comparison of the theoretical α -PbO (39) and the experimental α -PbO (Table 1 and Figure 1), the accuracies of the interatomic distances (R) and N between Pb and the first shell O backscatterers can be estimated. In this case, the accuracies are smaller than the confidence limits of the least-squares nonlinear fitting procedure. Thus, the accuracies can be inferred from the precisions given in Table 1. Similarly, the accuracies of R and N for second shell Al backscatterers can be inferred from the precision of the fits of the second shell Pb atoms in the α -PbO (20).

Results and Discussion

Pb XAS. Figure 1a shows the background subtracted k^3 weighted χ functions for the samples incubated for times of 1.5 h to 23 days and the α -PbO. A strong sinusoidal beat pattern typical of first neighbor O-shell backscattering is observed for all sorption samples. The existence of multiple frequencies due to second shell backscattering would result in dampening or additive amplitude effects on the peaks or the development of shoulders due to a distinct frequency from the major frequency. However, these characteristics are difficult to distinguish in the χ function when their contributions are small. The characteristic frequencies of the individual components that exist in the χ function are more easily observed by Fourier transforming the spectra into radial structure functions (RSF). Figure 1b shows the RSF (uncorrected for phase shift) for the different samples and the respective best fits that resulted from multiple shell fitting. Qualitative analysis of the χ structure and the RSF for the different samples do not reveal any significant differences between the samples incubated for different

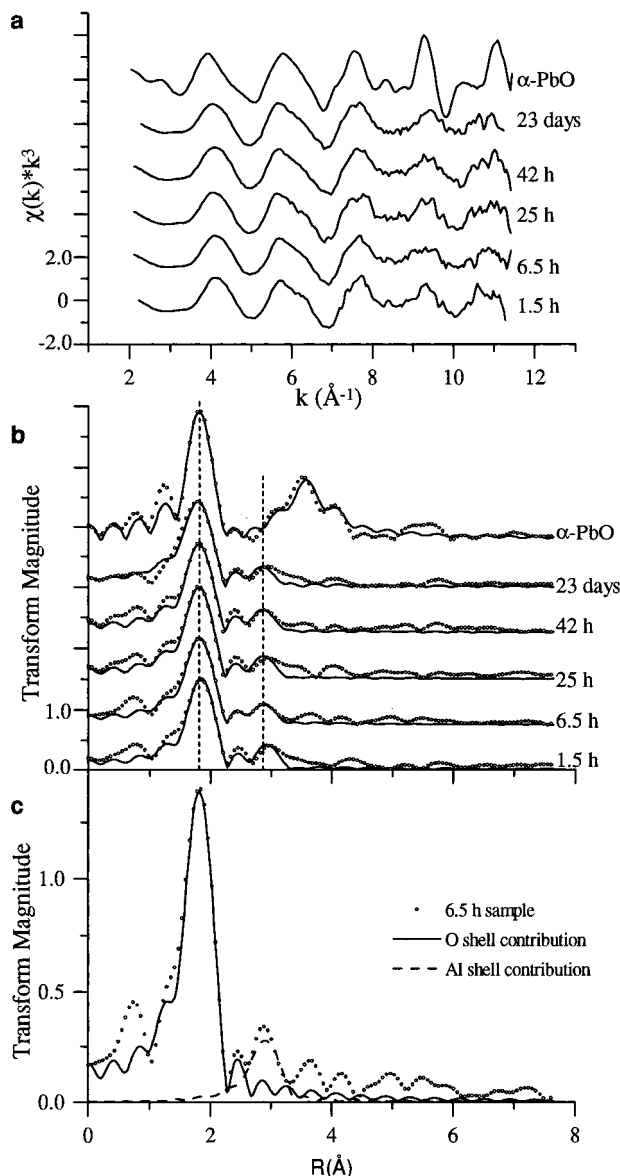


FIGURE 1. Results of the XAFS experiments. (a) k^3 weighted normalized χ -functions for samples incubated for different lengths of time and α -PbO (amplitude of α -PbO spectrum is one-half actual). (b) Fourier transforms (RSF) of the χ -function in panel a (amplitude of α -PbO spectrum is one-half actual). Vertical dashed lines are aligned at the center of the two major peaks used for fitting. The solid line is the theoretical multishell fit to the data; the dotted line represents the experimental data. (c) RSF of sample incubated for 6.5 h with the individual shell contributions.

lengths of time. The lack of the development of any major second shells in the region between 3.0 and 4.0 Å in the RSF (based on the position of Pb–Pb shells in the RSF of α -PbO in Figure 1b) suggests that a Pb surface precipitate is not occurring.

The best fits of the data were obtained by fitting two shells: the first shell containing an O atom and the second shell containing an Al atom. Attempts to fit Pb in the second shell, both with and without the Al atom, were unsuccessful. The fit of the theoretical RSF to the experimental RSF for Δk (Å⁻¹) = 3.6–11.3 and ΔR (Å) = 1.01–3.35 is shown in Figure 1b for the different sorption samples. The results of the fit are presented in Table 1. The peak centered at ~ 1.80 Å in the RSF can be fit with 1.86–2.23 O backscatterers at $R = 2.28$ –2.30 Å. The second peak centered at ~ 2.90 Å can be fit with 0.91–1.11 Al backscatterers at $R = 3.38$ –3.43 Å. The

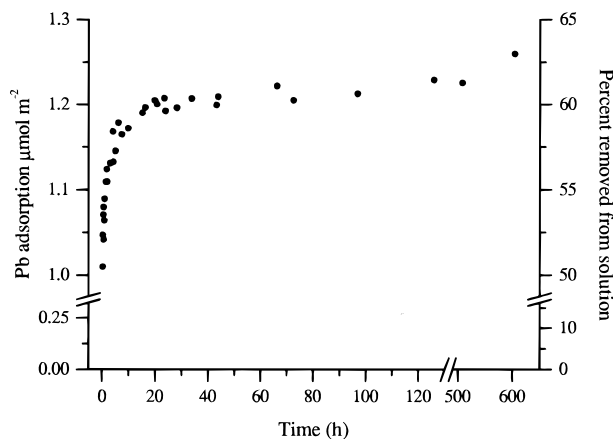


FIGURE 2. Lead adsorption kinetics on $\gamma\text{-Al}_2\text{O}_3$ at pH 6.50, $I = 0.1$ M, and $[\text{Pb}]_{\text{initial}} = 2.0$ mM, surface area = $100 \text{ m}^2 \text{ g}^{-1}$. Data points are from three separate experiments.

RSF and best fit for the $\alpha\text{-PbO}$ are included for comparison.

Individual contributions to the two shells for the sample incubated for 6.5 h are shown in Figure 1c. Three important points can be made from Figure 1c: (1) the two major peaks in the RSF of the raw data are reasonably modeled by backscattering from first shell O and a second shell Al; (2) the small peak centered at $\sim 2.45 \text{ \AA}$ in the raw spectra is not necessarily a contribution from another backscattering atom since it can be explained by the combined contributions from side lobes of the O and the Al backscatterers; and (3) various other small peaks located after the primary backscattering peak in the RSF exist that are most likely due to scattering from additional atoms present in small amounts in the second shell (e.g., Pb), combinations of side lobes from the two dominant peaks, noise in the data, and/or frequencies that exist in the spectra due to multiple scattering paths. Attempts to resolve point three by fitting were unsuccessful due to the low amplitude of the peaks and the limited capabilities of fitting routines when too many free variables are introduced.

The structural parameters obtained from the XAFS are similar to those presented by Bargar et al. (20), who hypothesized that the bonding coordination environment for Pb consisted of three hydroxyls arranged in a distorted trigonal pyramid (20). Using known Al–O bond distances [average from the literature = 1.91 \AA (20)] and experimental Pb–O distances (average $R = 2.29 \text{ \AA}$), the calculated maximum Pb–Al bond distance should be 3.42 \AA when Pb is sorbed as an inner-sphere complex sharing hydroxyl ligands on the edge of an octahedral complex (20). The average Pb–Al bond distance of all of the samples in these experiments is 3.40 \AA . Thus, we conclude that the majority of Pb in our experiments is adsorbed as an inner-sphere bidentate edge complex. Increasing incubation time had no noticeable effect on the local atomic structure of the sorbed Pb. The possibility of surface precipitation at pH 6.50 and surface loadings of $1.10\text{--}1.27 \mu\text{mol m}^{-2}$ can be ruled out since a significant peak was not observed in the RSF, nor were we able to successfully fit Pb as a backscattering atom using the multishell fitting procedure.

Adsorption Kinetics. The results of the adsorption kinetics experiment are presented in Figure 2. Within 15 min a very fast adsorption reaction occurred accounting for 76% of total adsorbed Pb. Following the initial fast reaction, the adsorption reaction continued for ~ 30 h, after which only a small amount of additional sorption occurred ($\sim 2.5\%$). After 600 h, $\sim 63\%$ of the Pb initially added to the suspension had been adsorbed. Attempts to fit the data with a linear

form of the steady-state first-order reaction equation were unsuccessful, providing evidence that the reaction kinetics data represent separate reaction mechanisms. Fast Pb adsorption reactions on $\gamma\text{-Al}_2\text{O}_3$ have been studied using relaxation kinetic methods (reaction times on the order of seconds) (40, 41). Results of these studies suggest that fast reactions are most likely a chemical reaction with surface sites on $\gamma\text{-Al}_2\text{O}_3$ that are readily accessible (40, 41). Secondary slow reactions have been observed for metal sorption on many different (hydr)oxides (3, 9, 11, 13–15). Hayes and Leckie (40) reported that sorption of Pb on goethite continued for times as long as hours to days. Similarly, Benjamin and Leckie (42) observed that sorption of several heavy metals (including Pb) on amorphous iron oxyhydroxide was initially fast followed by a much slower second step.

As mentioned above, there are three possible explanations for the slow reaction: diffusion to internal sites, surface precipitation, or adsorption to sites that have a slower reaction rate due to low affinity (9, 11, 13–15). In this experiment, a fourth possibility for the slow sorption reaction is the formation of additional sorption sites due to the slow transformation of $\gamma\text{-Al}_2\text{O}_3$ into a lower energy solid phase (43). Surface precipitation can be ruled out based on the XAFS results presented earlier. However, the other slow sorption mechanisms are difficult to isolate.

Diffusion-limited sorption is likely occurring since the $\gamma\text{-Al}_2\text{O}_3$ structure is a microcrystalline material consisting of small connected particles with a large internal surface (44, 45). In addition, the formation of stable aggregates during preequilibration can occur, creating physical barriers that restrict access to adsorption sites. The Schultze–Hardy rule predicts that for monovalent ions in a suspension of aluminum hydrous oxide the critical coagulation constant is 0.05 M (46). Since the $\gamma\text{-Al}_2\text{O}_3$ suspension was preequilibrated with an anion concentration well above this value ($\sim 0.1 \text{ M}$), coagulation is likely. Diffusion as a rate-limiting sorption mechanism was observed in the experiments of Papeis and colleagues (3, 47), who employed kinetic experiments and X-ray photon spectroscopy (XPS) to show that the slow adsorption reaction of Cd and selenite onto porous alumina is a diffusion-controlled reaction.

In addition to slow diffusion occurring, slow reactions with aluminol sites may also occur. Lead hydrolysis and association reactions are generally thought to be fast (40, 41). However, several different types of ligand sites exist on $\gamma\text{-Al}_2\text{O}_3$ (20), and sorption onto sites with large activation energies is possible (resulting in slower kinetics) (48).

It can be concluded that Pb adsorption kinetics are biphasic, that is, an initially fast reaction is followed by a slow reaction. In this paper, we have provided evidence that the slow sorption reaction is not a result of surface precipitation. However, the distinction between the other three mechanisms mentioned above would require additional experiments. The kinetic data in this paper do suggest that there exists a significant slow Pb adsorption reaction on $\gamma\text{-Al}_2\text{O}_3$. Thus, when making predictions based on equilibrium, this slow reaction step should be considered.

Desorption Experiments. The desorption behavior of Pb from $\gamma\text{-Al}_2\text{O}_3$ using the replenishment method is presented in Figure 3. The results show that the Pb is steadily removed from the surface with each replenishment. After four replenishments, the slope of the percent removed versus the number of replenishments decreases. This is likely due to the increased affinity by the surface for Pb as the adsorbed concentration decreases (nonlinear isotherm behavior). The replenishment experiments provide an indication of the strength of the Pb–surface bond. If the Pb is held strongly by the surface, little desorption would be expected over the time scale of the measurements due to an increased activation energy requirement. However, in this experiment 69% of

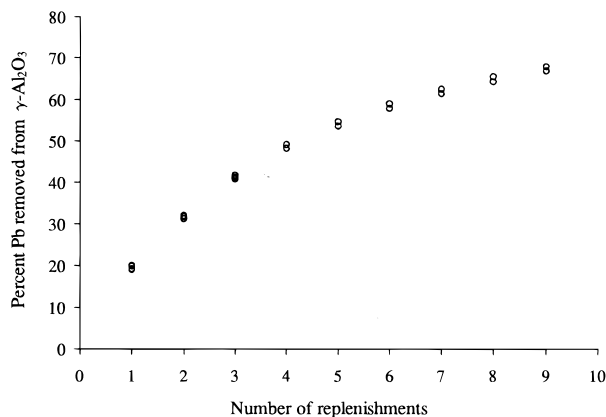


FIGURE 3. Desorption of Pb from $\gamma\text{-Al}_2\text{O}_3$ by replenishing background electrolyte every 24 h. Data points are from three separate experiments.

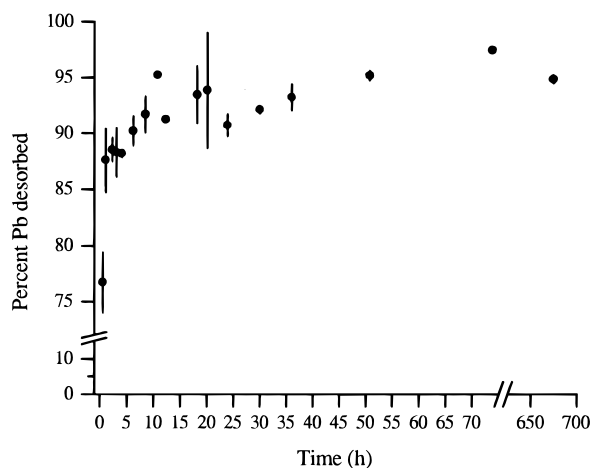
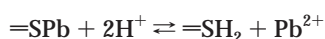


FIGURE 4. Lead desorption kinetics from $\gamma\text{-Al}_2\text{O}_3$ using Na-saturated resins, pH 6.50, $I = 0.1$ M. Error bars are standard deviations of three samples.

the sorbed Pb was removed after nine replenishments. It is likely that with additional replenishments all of the adsorbed Pb would be removed from the surface. Thus, we hypothesize that Pb is not forming strong bonds with $\gamma\text{-Al}_2\text{O}_3$ that would require large activation energies to break. It is important to note that the data in Figure 3 do not necessarily represent the actual Pb desorption behavior. If equilibrium was reached in each replenishment, then the results from the experiment would represent a reverse isotherm. If the system were far from equilibrium so that back reactions were insignificant, the data would represent the desorption kinetic behavior. Neither of these conditions is present in this experimental system, but this experiment does show that Pb is readily released from the surface, suggesting that the activation energy for this process is small.

One useful technique for evaluating desorption kinetics is to drive the desorption forward by removing the products to avoid back reactions, for example, removing Pb^{2+} from the simplified desorption reaction



where $=\text{S}$ is a surface site. This simplifies the desorption kinetics since back reactions are eliminated (49). The desorbed Pb can be removed from solution by using cation-exchange resins that have a high affinity for the ion being desorbed. Figure 4 shows the results of the desorption kinetics using a Na-saturated resin as a sink for $\text{Pb}(\text{aq})$ to eliminate back reactions. Similar to the adsorption kinetics,

the desorption kinetics show a biphasic type behavior; within 30 min 78% of the Pb is desorbed from the surface, followed by slow desorption continuing for 70 h, resulting in a recovery of 98% of the sorbed Pb. The mechanisms responsible for the fast and slow desorption kinetic behavior are likely the reverse reactions of the adsorption mechanisms; initially a fast desorption from sites readily available followed by a slow release from sites on the interior of the solid. This behavior suggests that diffusion-limited sorption is responsible for the slow sorption reaction.

Resins are often used in studies to examine the availability and potential leachability of ions in soils since they remove aqueous cations from solution (50, 51). In our experiments, the resin was able to remove all of the aqueous Pb, causing the surface to release all of the sorbed Pb in an attempt to reestablish equilibrium. The ease with which the Pb was removed from the surface of the $\gamma\text{-Al}_2\text{O}_3$ suggests that the bond between Pb and aluminol sites is weak as compared to the bond formed between Pb and the functional groups of the resin. Therefore, we hypothesize that adsorption onto aluminum (hydr)oxide minerals may not be a significant mechanism for Pb retention in systems where other sorbents exist that can complex Pb more strongly (e.g., organic matter, clays, and carbonates).

The complete desorption of Pb from the surface is surprising since it is commonly thought that the bonds formed in inner-sphere sorption are relatively strong and irreversible due to the higher activation energy required for desorption as compared to adsorption (48, 52, 53). However, these desorption experiments show that Pb is readily released from a surface with which it has formed a direct chemical bond. Gunneriusson et al. and Ainsworth et al. (54, 55) also found that Pb adsorbed onto goethite and hydrous iron oxide, respectively, is reversible with respect to pH.

The results of this study suggest three important points that will improve the capabilities of researchers to predict the fate of Pb in the environment: (1) the molecular environment of Pb sorbed onto $\gamma\text{-Al}_2\text{O}_3$ is stable when allowed to incubate for long periods and does not involve the formation of Pb surface precipitates. (2) Pb adsorption is characterized by fast and slow reaction steps (after 30 h the reaction has slowed considerably). (3) Pb adsorption appears to be reversible provided that Pb desorption is carried out for a long enough time (~ 3 d in this case).

Acknowledgments

Thanks are extended to the Staff at beamline X-11A, Dr. J. McBreen for the lead oxide sample, Dr. B. Boyanov and Professor D. Sayers for assistance in data analysis, E. Elzinga and Dr. R. Ford for critical comments on the manuscript, and Professor L. Katz for insightful discussion. D.G.S. is grateful for a University of Delaware Competitive Fellowship. We would also like to acknowledge the financial contribution to this project by the DuPont Company.

Literature Cited

- (1) Sposito, G. *The Chemistry of Soils*; Oxford University Press: New York, 1989.
- (2) Steinfeld, J. I.; Francisco, J. S.; Hase, W. L. *Chemical Kinetics and Dynamics*; Prentice Hall: Englewood Cliffs, NJ, 1989.
- (3) Papelis, C.; Roberts, P. V.; Leckie, J. O. *Environ. Sci. Technol.* **1995**, *29*, 1099–1108.
- (4) Sparks, D. L. *Environmental Soil Chemistry*; Academic Press: San Diego, 1995.
- (5) Harter, R. D. In *Rates of Soil Chemical Processes*; Sparks, D. L., Suarez, D. L., Eds.; Soil Science Society of America: Madison, WI, 1991; Vol. 27, pp 135–149.
- (6) Verburg, K.; Baveye, P. *Clays Clay Miner.* **1994**, *42*, 207–220.
- (7) Lehman, R. G.; Harter, R. D. *Soil Sci. Soc. Am. J.* **1984**, *48*, 769–772.
- (8) Sparks, D. L. *Kinetics of Soil Chemical Processes*; Academic Press: San Diego, CA, 1989.

- (9) Fuller, C. C.; Davis, J. A.; Waychunas, G. A. *Geochim. Cosmochim. Acta* **1993**, *57*, 2271–2282.
- (10) Smith, J. T.; Comans, R. N. J. *Geochim. Cosmochim. Acta* **1996**, *60*, 995–1004.
- (11) Axe, L.; Anderson, P. R. *J. Colloid Interface Sci.* **1997**, *185*, 436–448.
- (12) Scheidegger, A. M.; Strawn, D. G.; Lambie, G. M.; Sparks, D. L. *Geochim. Cosmochim. Acta*. In press.
- (13) Loehr, R. C.; Webster, M. T. *J. Soil Contam.* **1996**, *5*, 361–393.
- (14) Scheidegger, A. M.; Sparks, D. L. *Chem. Geol.* **1996**, *132*, 157.
- (15) Towle, S. N.; Bargar, J. R.; Brown, G. E., Jr.; Parks, G. A. *J. Colloid Interface Sci.* **1997**, *187*, 62–82.
- (16) Chisholm-Brause, C. J.; Hayes, K. F.; Roe, A. L.; Brown, G. E., Jr.; Parks, G. A.; Leckie, J. O. *Geochim. Cosmochim. Acta* **1990**, *54*, 1897–1909.
- (17) Roe, A. L.; Hayes, K. F.; Chisholm-Brause, C.; Brown, G. E., Jr.; Parks, G. A.; Hodgson, K. O.; Leckie, J. O. *Langmuir* **1991**, *7*, 367–373.
- (18) Bargar, J. R.; Towle, S. N.; Brown, G. E., Jr.; Parks, G. A. *Geochim. Cosmochim. Acta* **1996**, *60*, 3541–3547.
- (19) Manceau, A.; Bosset, M.-C.; Sarret, G.; Hazemann, J.-L.; Mench, M.; Cambier, P.; Prost, R. *Environ. Sci. Technol.* **1996**, *30*, 1540–1552.
- (20) Bargar, J. R.; Brown, G. E., Jr.; Parks, G. A. *Geochim. Cosmochim. Acta* **1997**, *61*, 2617–2637.
- (21) Hesterberg, D.; Sayers, D. E.; Zhou, W.; Plummer, G. M.; Robarge, W. P. *Environ. Sci. Technol.* **1997**, *31*, 2840–2846.
- (22) Waychunas, G. A.; Rea, B. A.; Fuller, C. C.; Davis, J. A. *Geochim. Cosmochim. Acta* **1993**, *57*, 2251–2269.
- (23) Hunter, D. B.; Bertsch, P. M. *Environ. Sci. Technol.* **1994**, *28*, 686–691.
- (24) O'Day, P.; Brown, G. E., Jr.; Parks, G. A. *J. Colloid Interface Sci.* **1994**, *165*, 269–289.
- (25) O'Day, P. A.; Chisholm-Brause, C.; Towle, S. N.; Parks, G. A.; Brown, G. E., Jr. *Geochim. Cosmochim. Acta* **1996**, *60*, 2515.
- (26) Valcheva, M. L.; Davidova, N.; Weiss, A. H. *J. Mater. Sci.* **1995**, *30*, 737–743.
- (27) Goldberg, S.; Davis, J. A.; Hem, J. D. In *The Environmental Chemistry of Aluminum*; Sposito, G., Ed.; CRC Press: Boca Raton, FL, 1995; pp 271–332.
- (28) Hohl, H.; Stumm, W. *J. Colloid Interface Sci.* **1976**, *55*, 281–287.
- (29) Kinniburgh, D. G. *Soil Sci. Soc. Am. J.* **1976**, *40*, 796–799.
- (30) Davis, J. A. *J. Colloid Interface Sci.* **1978**, *67*, 90–107.
- (31) Bargar, J. R.; Towle, S. N.; Brown, G. E., Jr.; Parks, G. A. *J. Colloid Interface Sci.* **1997**, *185*, 473–492.
- (32) Knozinger, H.; Ratnasamy, P. *Catal. Rev.—Sci. Eng.* **1985**, *17*, 31–70.
- (33) Good, M. E.; Winget, G. D.; Winter, W.; Connolly, T. N.; Izawa, S.; Singh, R. M. M. *Biochemistry* **1966**, *5*, 467–477.
- (34) Baeyens, B.; Bradbury, M. H. *A Quantitative Mechanistic Description of Ni, Zn and Ca Sorption on Na-Montmorillonite*; Report PSI Ber. 95-11; Paul Scherrer Institut: Villigen, Switzerland, 1995.
- (35) Lytle, F. W.; Gregor, R. B.; Sandstorm, D. R.; Marques, E. C.; Wong, J.; Spiro, C. L.; Huffman, G. P.; Huggins, F. E. *Nucl. Instrum. Methods Phys. Res.* **1984**, *226*, 542–548.
- (36) Bouldin, C.; Furenid, L.; Elam, T. *Phys. B* **1995**, *208/209*, 190–192.
- (37) Stern, E. A. In *X-ray Absorption: Principles, Applications, and Techniques of EXAFS, SEXAFS, and XANES*; Koningsberger, D. C., Prins, R., Eds.; Wiley: New York, 1988; pp 3–51.
- (38) Zabinski, S. I.; Rehr, J. J.; Ankudinov, A. *Phys. Rev. B* **1997**, *52*, 2995–3009.
- (39) Leciejewicz, J. *Acta Crystallogr.* **1961**, *14*, 1304.
- (40) Hayes, K. F.; Leckie, J. O. In *Geochemical Processes at Mineral Surfaces*; Davis, J. A., Hayes, K. F., Eds.; American Chemical Society: Washington, DC, 1986; Vol. 323, pp 115–141.
- (41) Yasunaga, T.; Ikeda, T. In *Geochemical Processes at Mineral Surfaces*; Davis, J. A., Hayes, K. F., Eds.; American Chemical Society: Washington, DC, 1986; Vol. 323, pp 231–253.
- (42) Benjamin, M. M.; Leckie, J. O. *J. Colloid Interface Sci.* **1981**, *79*, 209–221.
- (43) Dyer, C.; Hendra, P. J. *Spectrochim. Acta* **1993**, *49A*, 691–705.
- (44) Shriver, D. F.; Atkins, P.; Langford, C. H. *Inorganic Chemistry*; W. H. Freeman and Company: New York, 1994.
- (45) Kinniburgh, D. G.; Jackson, M. L. In *Adsorption of Inorganics at Solid-Liquid Interfaces*; Anderson, M. A., Rubin, A. J., Eds.; Ann Arbor Science: Ann Arbor, 1981; pp 91–160.
- (46) Sposito, G. *The Surface Chemistry of Soils*; Oxford University Press: New York, 1984.
- (47) Papelis, C. *Environ. Sci. Technol.* **1995**, *29*, 1526–1533.
- (48) Strawn, D. G.; Sparks, D. L. In *The Fate and Transport of Trace Metals in the Environment*; Selim, H. M., Iskandar, A., Eds.; Ann Arbor Press: Ann Arbor, MI, 1998 (in press).
- (49) Amacher, M. C. In *Rates of Soil Chemical Processes*; Sparks, D. L., Suarez, D. L., Eds.; Soil Science Society of America: Madison, WI, 1991; Vol. 27, pp 19–59.
- (50) Sadusky, M. C.; Sparks, D. L.; Noll, M. R.; Hendricks, G. J. *Soil Sci. Soc. Am. J.* **1987**, *51*, 1460–1465.
- (51) Skogley, E. O.; Dobermann, A. *J. Environ. Qual.* **1996**, *25*, 13–24.
- (52) McBride, M. M. In *Interactions at the Soil Colloid-Soil Solution Interface*; Bolt, G. H., Boodt, M. F. D., Hayes, M. H. B., McBride, M. B., Eds.; Kluwer Academic Publishers: Dordrecht, 1991; Vol. 190, pp 149–176.
- (53) McBride, M. M. *Environmental Chemistry of Soils*; Oxford University Press: New York, 1994.
- (54) Ainsworth, C. C.; Pilon, J. L.; Gassman, P. L.; Van Der Sluys, W. G. *Soil Sci. Soc. Am. J.* **1994**, *58*, 1615–1623.
- (55) Gunneriusson, L.; Lovgren, L.; Sjoberg, S. *Geochim. Cosmochim. Acta* **1994**, *58*, 4973–4983.

Received for review February 16, 1998. Revised manuscript received May 28, 1998. Accepted June 25, 1998.

ES9801521